Title
THE EFFECTS OF QUARK COMPOSITENESS AT THE SSC

Authors
Bars, I.
Hinchliffe, I.

Publication Date
1985-07-01

LBL-19890
Preprint

Lawrence Berkeley Laboratory
UNIVERSITY OF CALIFORNIA

Physics Division

Submitted for publication

THE EFFECTS OF QUARK COMPOSITENESS AT THE SSC

I. Bars and I. Hinchliffe

July 1985

Prepared for the U.S. Department of Energy under Contract DE-AC03-76SF00098

LBL-19890

DISCLAIMER

July 1985

LBL-19890
USC-85/21

THE EFFECTS OF QUARK COMPOSITENESS AT THE SSC *

Itzhak Bars

Physics Department
University of Southern California
Los Angeles, CA 90089-0484
and
Ian Hinchliffe

Lawrence Berkeley Laboratory
University of California
Berkeley, CA 94720

ABSTRACT

The effects of composite quarks on jet cross-sections at the SSC is discussed with particular emphasis upon the rates for jet energies above the composite scale. One main conclusion is that compositeness physics dominates other exotic physics if the compositeness scale is in the SSC range. Different composite models are compared in order to examine whether discrimination between them is possible.

*This work was supported by the Director, Office of Energy Research, Office of High Energy and Nuclear Physics, Division of High Energy Physics of the U.S. Department of Energy under Contract DE-AC03-7600098, and DE–FG03–84ER40168, and the USC Faculty Research and Innovation Fund.

In this paper we consider the consequences of quark compositeness on production rates at the SSC. Previous discussions of such composite effects have concentrated upon the effects of the following four-Fermi interaction between quarks.[1]

$$\pm \frac{G}{2\Lambda^2}\,\bar{\psi}A\psi\,\bar{\psi}B\psi \qquad (1)$$

This form is valid so long as the momentum transfer between the quarks is less than the scale Λ which characterises the scale of the new interactions which are responsible for the binding of the preonic constituents of quarks. The coupling constant G determines the strength of the interaction between the preons. The detailed form of the interaction (i.e. the Dirac structure present in eq. 1) depends upon the details of the binding interaction. If we take a V-A form for the interaction and set $G/4\pi \approx 1$ then the current limit on Λ from the $Sp\bar{p}S$ is $\sim 1/2\ TeV^2$. There is a better limit on the scale responsible for lepton compositeness from searching for the effects of a four-electron vertex in Bhabha scattering[3]. The SSC may be sensitive to values of Λ as large as 20TeV.[4]

What happens if Λ is of the order of a few TeV? Then the form given in Eq. 1 is not a valid approximation at SSC energies since momentum transfers in quark-quark scattering can exceed Λ. We need a model for the interactions of strongly bound objects (quarks) above the interaction scale. This is a familiar problem in hadronic physics when one attempts to create a model of hadron-hadron scattering with momentum transfers of order a few GeV. For hadrons we have a theory (QCD) which describes the interactions of quarks and consequently hadrons, but at this time lack the methods to extract predictions which can be tested. Instead, a phenomenology of hadronic interactions has been developed based on Regge theory and duality.[5] Amplitudes for hadronic scattering can be written which satisfy known properties of QCD (e.g. flavor conservation), are consistent with unitarity bounds at high energy and satisfy the correct crossing properties.

In the case of quark substructure, the fundamental theory is assumed to be similar to QCD except for modifications that lead to chiral symmetry conservation and hence to small mass composite quarks and leptons. Many models have been proposed but there are outstanding questions. For example we do not know a priori whether quarks and leptons have common constituents. Even if a detailed fundamental theory existed we still lack the methods of solving the strongly bound state problems, as in QCD. However, by analogy to QCD we may draw parallels between composite quarks and leptons and composite hadrons. Using such analogies

and phenomelogically reasonable ideas in hadron scattering, a detailed model of composite quark-quark an quark–gluon scattering was proposed.[6,9] The form that we shall use[6] will satisfy the constraints of unitarity bounds and crossing and will be varied in an attempt to determine whether or not it is possible to distinguish between different models of compositeness.

The amplitude for quark quark scattering will contain terms due to the exchanges of strongly interacting heavy bound states of the preons with mass of order Λ. (This is analagous to the exchange of the ρ in $\pi - \pi$ scattering.) For definiteness we will discuss quark-anti-quark scattering, the quark–quark crossing. In this case one would expect an s-channel singularity at the mass of the first heavy vector meson (M_v). Since we want to discuss an energy range of order M_V and larger, the amplitude should describe the resonance and Regge region, in analogy to hadronic physics. Assuming that confinement of preons is similar to confinement of quarks and therefore that stringlike flux configurations are responsible for an approximate duality principle and Regge behavior, the amplitude can be parametrized[6] in the Veneziano[7] form

$$B_{st} = \frac{g_v^2 \alpha'}{4} \frac{\Gamma(1-\alpha(s))\,\Gamma(1-\alpha(t))}{\Gamma(2-\alpha(s)-\alpha(t))} \tag{2}$$

Here g_v is the strength of the coupling between the preons. We take the following form for the fermionic Regge trajectory $\alpha(s)$

$$\alpha(s) = \frac{1}{2} + \alpha' s(1 + i\gamma) \tag{3}$$

This is constrained so that there is a massive spin 1 particle of mass M_v (analogous to the ρ meson in QCD), i.e. $Re[\alpha(M_v^2)] = 1$. Assuming the trajectory has intercept 1/2 (again by analogy with QCD) we find $\alpha' = (2\,M_v^2)^{-1}$. The imaginary part in Eq. 3 has been chosen so that the first resonance has width $\Gamma = \gamma M_v$. We will vary $\gamma = \frac{1}{20}, \frac{1}{5}, \frac{1}{2}$. Near the first s-channel pole the amplitude reduces to (see Figure 1)

$$B_{st} \overset{s \to M_v^2}{\longrightarrow} \frac{g_v^2}{4(s - M_v^2 + i\Gamma M_v)} \tag{4}$$

This can be compared with the form of the ρ^0 pole in $p\bar{p} \mapsto n\bar{n}$, where g_v^2 is replaced by $g_{\rho NN}$. We will use this analogy to estimate the strong coupling

$$g_v^2 \cong g_\rho^2 = 8\pi \tag{5}$$

In the limit of very small s the amplitude reduces to

$$B_{st} \to -\frac{\pi g_v^2}{8M_v^2} \tag{6}$$

i.e. the same four fermi form as given above (Eq. 1), with $|G| = 4\pi$ and $\Lambda = \sqrt{8/\pi}\, M_v \cong 1.6 M_v$.

It is necessary to include an additional term in the amplitude to take account of the exchange of vacuum quantum numbers in the t-channel. This "Pomeron" term is given by

$$P(s,t) = \frac{2\pi g_p^2}{M_v^2} \frac{1 + \exp(i\pi\alpha_p(t))}{\cos\left(\frac{\pi}{2}\alpha_p(t)\right)} \left(\frac{s}{4M_v^2}\right)^{\alpha_p(t)-1} \tag{7}$$

with the trajectory

$$\alpha_P(t) = 1 + \alpha' t \tag{8}$$

We can normalize the coupling g_p by using the optical theorem to determine the total cross section

$$\sigma_{tot} = \frac{1}{s} ImP(s,0) \overset{s \to \infty}{\longrightarrow} \frac{4\pi g_p^2}{M_v^2} \tag{9}$$

On the basis of the geometrical model we would expect this cross-section to be of order

$$\sigma_{tot} = 2\pi R^2 \tag{10}$$

where R is the size of the quark. Since $M_v \sim 3/R$ (in QCD at least) we would expect g_p to be of order 1-4. In what follows we shall keep g_v fixed and vary g_p.

Unfortunately, the pomeron form will violate unitarity bounds if it is crossed naively. To avoid this problem in numerical integrations we have replaced it by a phenomenological expression that is crossing symmetric and can be used at large values of both s and t.

$$P_{st} = \frac{2\pi g_p^2}{M_v^2} \frac{1 + \exp(i\pi\alpha_p(t))}{\cos(\frac{\pi}{2}\alpha_p(t))} \frac{\Gamma\left(c + \frac{\alpha'}{2}||s| - |t||\right)}{\Gamma\left(c + \frac{\alpha'}{2}||s| + |t||\right)} \tag{11}$$

For large s and small negative t (11) reduces to (7). The constant c is undetermined; it will be varied in what follows.

If we write the cross-section for quark-anti-quark scattering in the form

$$\frac{d\sigma}{dt} = \frac{1}{16\pi s^2} |M|^2 \tag{12}$$

then the quantity $|M|^2$ is given as follows.[6] For the processes $q_i\bar{q}_i \to q_i\bar{q}_i$, namely, $u\bar{u} \to u\bar{u}$, $d\bar{d} \to d\bar{d}$, $s\bar{s} \to s\bar{s}$, $c\bar{c} \to c\bar{c}$, $t\bar{t} \to t\bar{t}, b\bar{b} \to b\bar{b}$, we have

$$\begin{aligned}
|M|^2 = \Big\{ & u^2 \left[\frac{4}{9} g^4 \left(\frac{1}{s^2} - \frac{1}{3st} \right) + \frac{16}{9s} g^2 Re(xB_{st} + P_{st}) \right. \\
& \left. + \frac{8}{3} x^2 |B_{st}|^2 + \frac{16}{3} x Re(B_{st}^* P_{st}) + 2|P_{st}|^2 + \frac{2}{3} Re(P_{st}^* P_{ts}) \right] \\
& + s^2 \left[\frac{4}{9} \frac{g^4}{t^2} \pm \frac{16}{9} z \frac{g^2}{t} Re(B_{st}) + 2(y^2 + z^2 + \frac{2}{3} yz) |B_{st}|^2 \right. \\
& \left. + \frac{4}{3}(3y + z) Re(B_{st}^* P_{st}) + 2|P_{st}|^2 \right] \Big\} \\
& + \{s \leftrightarrow t\}
\end{aligned} \tag{13}$$

where the parameters x, y, z and the sign ± depend on models as described in Ref. (6). These parameters for 4 classes of models are listed in Table 1. For the processes of the type $q_i\bar{q}_j \to q_i\bar{q}_j$ with i≠j, as listed in Table 1, we have

$$\begin{aligned}
|M|^2 = & u^2 \left\{ \frac{4}{9} \frac{g^4}{s^2} + \frac{16}{9} \frac{g^2}{s} x_H Re(B_{st}) + 2\left(x_H^2 + x_V^2 + \frac{2}{3} x_H x_V \right) |B_{st}|^2 \right. \\
& \left. + \frac{4}{3}(3x_V + x_H) Re(B_{st}^* P_{ts}) + 2|P_{ts}|^2 \right\} \\
& + 2s^2 (y_H^2 + y_V^2 + 2y_H y_V) |B_{st}|^2 \\
& + t^2 \left\{ \frac{4}{9} \frac{g^4}{s^2} \pm \frac{16}{9} z_H \frac{g^2}{s} Re(B_{st}) + 2(z_H^2 + z_V^2 + 2z_H z_V) |B_{st}|^2 \right. \\
& \left. + \frac{4}{3}(3z_V + z_H) Re(B_{st}^* P_{ts}) + 2|P_{ts}|^2 \right\}
\end{aligned} \tag{14}$$

Again, the parameters $x_H, x_V, y_H, y_V, z_H, z_V$ are model dependent as in Table 1.

In addition to the processes listed in the table, there are $q_i\bar{q}_j \to q_i\bar{q}_j$ reactions that are obtained by crossing symmetry, such as $u\bar{d} \to u\bar{d} \cdots, u\bar{c} \to u\bar{c} \cdots, u\bar{s} \to$

$u\bar{s} \cdots . |M|^2$ for these reactions is obtained from (14) by interchanging $s \leftrightarrow t$ and using the parameters of the crossing symmetric reaction in Table 1. There are also family conserving reactions of the type $q_i\bar{q}_j \to q_k\bar{q}_\ell$, as listed in Table 1.

$$|M|^2 = 2\left(x_H^2 + x_V^1 + \frac{2}{3} x_V x_H \right) (u^2 + t^2) |B_{st}|^2 \tag{15}$$

Finally there are the crossing symmetric reactions $u\bar{d} \to c\bar{s}$ etc, for which s and t should be interchanged in (15). Notice that there is no QCD term in the expression 15, while in (13, 14) the terms proportional to g are due to QCD. All possible channels, including the family changing channels, are included in the figures presented below. Dangerous flavor changing neutral currents such as $K_L \to \mu e$ can be avoided by choosing models with the correct assignment of composite states to observed quarks and leptons, so that M_v can be in the range accessible at the SSC (see Ref. 8). The models we investigate here allow $M_v \geq 1 - 2\ TeV$, where the limit comes from Bhabba scattering[3] and $e\bar{e} \to \mu\bar{\mu}$, assuming that both quarks and leptons are composite.

Before we can proceed to examine the consequences of the cross-sections we have to decide whether or not to modify the partonic cross-sections which involve gluons. We will assume that the gluon is not a composite object, in which case composite effects in gluon quark scattering can be manisfest only via graphs of the type shown in Figure 2. This is analogous to the effects of strong interactions on photon-nucleon scattering, which can be discussed in terms of e.g. vector meson dominance or other more general form factors. We have the following form[9] for $|M|^2$ $(q\bar{q} \to gg)$

$$\begin{aligned}
|M|^2 = \frac{8}{3} g^2 \Big[& (t^2 + u^2) \left| \frac{A_s}{s} \right|^2 - \frac{4}{9} |P(t,s) + A(s,t)|^2 \\
& - \frac{4}{9} tu |P(u,s) + A(s,u)|^2 \Big]
\end{aligned} \tag{16}$$

with

$$A_s = \frac{1}{\sqrt{\pi}} \frac{\Gamma(1 - \alpha(s))}{\Gamma(5/2 - \alpha(s))} \quad ; \quad \alpha(s) = \frac{1}{2} + \alpha' s(1 + i\gamma)$$

$$A(s,t) = -\alpha'(1 + i\gamma) \frac{\Gamma(1 - \alpha(s))\, \Gamma(1/2 - \alpha(t))}{\Gamma(3/2 - \alpha(s) - \alpha(t))}$$

Here $\alpha(s)$ is the vector meson trajectory while $\alpha(t)$ is the fermion trajectory, which unlike QCD, is expected to be almost degenerate with the meson trajectory.[6]

The matrix elements for $gg \to q\bar{q}$ and $gq \to gq$ are obtained by crossing viz.

$$|M|^2(s,t,u)_{gg\to q\bar{q}} = \frac{9}{64}|M|^2(s,t,u)_{q\bar{q}\to gg}$$
$$|M|^2(s,t,u)_{gq\to gq} = \frac{3}{8}|M|^2(t,s,u)_{q\bar{q}\to gg}$$

This reduces to the usual QCD result in the limit $M_v \to \infty$. Note that the gluon coupling g appears here instead of the strong coupling constant g_v of Eq. 2 for the quark quark case. This reflects the elementary nature of the gluon. Since $g^2/4\pi \approx 0.1$ is negligible compared to $g_v^2/4\pi \approx 2$, we should expect that gluons are not important if M_v is a few TeV. Despite the abundance of gluonic partons, our plots confirm this expectation (see below). Thus, unless it proves possible to distinguish quark and gluon jets experimentally, gluons are negligible from the point of view of exploring compositeness.

We could also include a term to model composite effects in gluon gluon scattering (Figure 3)

$$|M|^2 = \frac{9}{2}g^4\left[3|1+A(s,t,u)|^2 - tu\left|\frac{1}{s}+A(t,u)\right|^2\right.$$
$$\left. - su\left|\frac{1}{t}+A(s,u)\right|^2 - st\left|\frac{1}{u}+A(s,t)\right|^2\right] \qquad (17)$$

The form factors A(s,t,u) etc. must vanish as $M_v \to \infty$, so that this expression reduces to the usual QCD form in the limit $M_v \to \infty$. Because of the higher powers of g, this contribution is negligible and we do not need to specify the unknown form factors.

We shall now illuminate the effects of compositeness upon jet cross sections at the SSC. The structure functions of Ref. 4 are used in obtaining these physical cross-sections. In Figure 4 we show the cross section for the production of a jet at rapidity y = 0 as a function of the transverse momentum. We have taken a large $g_p = 3$ and c = 1 (see Eq. 11) and have used model 1 with the +/− sign taken to be +. All figures are for pp interactions at center of mass energy of 40 TeV. We have used $M_v = 3\ TeV$. The contributions of the different final states $q\bar{q}, gq, gg$ as well as the sum are shown separately. As expected, the contribution from gluons is small once the composite scale is reached. Figure 5 shows the total rate at different values of M_v.

For the set of parameters shown in Figs. 4-5 the pomeron term is dominant and consequently it is very difficult to discriminate between different models. Figure 6 shows model 3 with M_v = 3, 6, 10 and 30 Tev. (All other parameters are unchanged.) Comparison with Figs. 4-5 reveals little difference. The pomeron contribution has little structure hence the rather smooth cross-sections which result when it is dominant. The constant c is not relevant provided that it is of order one.

In the case of e.g. πp scattering in QCD the pomeron contribution is not dominant, otherwise the Δ resonance would not be seen clearly. It is reasonable therefore to consider the effect of a smaller pomeron contribution to the composite structure. The effect of reducing g_p to 1.0 is shown in Fig. 7. The structure is due to the resonance present in the amplitude Eq. 2. Figures 8, 9, and 10 show models 2, 3, and 4. Some discrimination among models may now be possible but it is difficult to imagine how the detailed structure of the compositeness could be determined unless it proved possible to distinguish jets produced by different quark flavors. We have not shown the effect of the–choice for the +/− in Eq. 13. Its effect is small even when g_p is small.

More structure can be extracted by studying the cross-section as a function of the jet pair mass. This cross-section is shown for model 1 in Figure 11 and for model 2 in Figure 12. Little discrimination among models is possible. It is clear that if $g_p << 1$ the resonance structure in these plots becomes more prominent and consequently discrimination among models may become possible.

We now turn to the width parameter $\gamma = \Gamma/M_v$ appearing in the Regge trajectory. There are several considerations that require attention.[10] At low energies, $\hat{s}, \hat{t} < M_v^2$, dimensional analysis makes it apparent that 2 body final states dominate $q\bar{q}$ scattering. When $\hat{s} \geq M_v^2$ we may suspect that multibody final states may begin to play the dominant role. We argue that multibody final states can emerge only when the preons involved in $q\bar{q}$ scattering are forced apart with sufficient energy ($\sqrt{\hat{s}} >> M_v$) that the precolor string, whose tension is measured by $\alpha' = (2M_v^2)^{-1}$, is forced to break more then once. We can learn by making analogies to QCD strings, whose tension is $\alpha' \sim (1GeV^2)^{-1}$. We consider data from e^+e^- collisons where the multiplicity of pions in $e^+e^- \to \gamma^* \to n\pi$ is $< n > \sim 2 - 2.5$ for $\sqrt{s} \leq$ 2-3 GeV, and rising like $< n > \approx 2 + b\ln(\alpha' s)$ with a small value of b. Thus, 2 body final states dominate at lower energies. This can be interpreted in terms of the QCD string prefering to make as few splits as possible when it is not forced to be too long by energetic quarks. This conclusion is also supported by the dom-

inance of $\rho \rightarrow 2\pi$ over $\rho \rightarrow 4\pi$ decay. Indeed in the decay of a heavy particle phase space suppression for massless multibody final states is enormous (see Ref. 11) and can only be overcome by a rapid increase in the multiplicity of diagrams (as in perturbation theory, which is not applicable here) or string breakings that contribute. Evidently these multiple string breakings do not occur in low energy QCD. By analogy, i. e. due to absence of multiple string breaking and the added enormous phase space suppression, we argue that preon-preon resonances at M_v (analogous to rho in QCD) would prefer to decay predominantly to two body final states consisting of quarks and leptons. Thus, the width Γ/M_v can be estimated by using 2 body final states and the coupling constant at the resonance Eq. (4). For a one channel partial decay $\Gamma_{1-channel} \approx M_v/8$. However, each heavy composite may decay into several 2-body final states depending on its quantum numbers derived from the preons. In the models we consider the number of final states range from 1 up to 48 depending on the quantum-numbers.[10] Consequently it is possible to have total widths ranging from $M_v/8$ up to $6M_v$ for the various heavy resonances. In our estimates we have used the values $\gamma = 0.2$ and 0.5 and noticed that for larger values of γ the resonance structure essentially disappears, as seen by comparing Figs. 12 and 13. We believe that the model dependent γ is not small enough for resonance structure to be striking, however, the possibility of a small γ should not be totally discarded.

The cross-sections due to composite effects are much larger than those due to other exotic physics with the same characteristic mass scale. This is a consequence of the larger strong coupling and of the behavior of the partonic cross section which ceases to fall as $\hat{s}_1$ once the threshold M_v had been crossed ($\hat{s}$ is the partonic center of mass energy squared.) There is little prospect of confusing compositeness with other new physics if the compsiteness scale is in the SSC range.

The case of large Λ or M_v was discussed in Ref. 4. A comparison of our results with Ref. 4 using $G = 4\pi$ and $\Lambda = \sqrt{8/\pi}M_v$ (see above) reveals that for $s << \Lambda$ our rates are larger than those of Ref. 4. This is due to the presence of a pomeron and more channels in our case: Ref. 4 did not include channels of the type $u\bar{u} \rightarrow c\bar{c}$ etc. With a small pomeron ($g_p = 1$) if we use the criteria of Ref. 4 to determine what maximum values of M_v(or Λ) are accessible at the SSC we will obtain slightly higher values. However, if M_v is only a few TeV, with $s \approx \Lambda$ or $s > \Lambda$ our results completely modify Ref. 4.

We have discussed composite effects only in two jet final states. Once the com-

posite threshold has been crossed it is to be expected that multi-jet cross-sections will depart radically from their QCD behavior. An estimate is inevitably model dependent, but their measurement will give valuable insight into the physics of the preons. If $\hat{s}$ is not considerably larger that M_v^2, our comments on string splitting above indicate that we should not expect multijet cross sections to dominate the total cross section. In that case the cross sections presented here already form a substancial part of the total cross section. It is also possible that leptons and quarks could share the same constituents, in which case the dilepton cross section will increase by several orders of magnitude compared to Drell-Yan production. This point will be investigated elsewhere.[10]

Acknowledgments

This work was supported by the Director, Office of Energy Research, Office of High Energy and Nuclear Physics, Division of High Energy Physics of the U.S. Department of Energy under Contracts DE-AC03-76SF00098, and DE-FG03-84ER, 40168, and the USC Faculty Research and Innovation fund.

References

1. E. Eichten, K. D. Lane and M. Peskin, Phys. Rev. Lett. 45, 255 (1980).
2. J. Hanson, Proc of 4th Topical Workshop on $p\bar{p}$ collider physics. Edited by H. Hanni and J. Schacker, CERN 84-09 (1984).
3. R. Brandelik et al., Phys. Lett. 117B 365 (1982).
4. E. Eichten, et al., Rev. Mod. Phys. 56 579 (1984).
5. See for example, M. Jacob, Physics Report C.
6. I. Bars in Proc. of 1984 DPF Summer Study on the Design and Utilization of the SSC. Editor, R. Donaldson and J. Morfin, FNAL (1985), p. 38.
7. G. Veneziano, Nucl. Phys. (1968).
8. I. Bars, Proc. of the 1984 DPF Summer Study on the Design and Utilization of the SSC, Ed. R. Donaldson and J. Morfin, FNAL(1985), p. 832.
9. C. Albright and I. Bars Proc. 1984 DPF Summer Study on the Design and Utilization of the SSC. Ed. R. Donaldson and J. Morfin, FNAL (1985), p. 34.
10. I. Bars, J. Gunion, M. Kwan, preprint USC-85/022.
11. I. Bars, M. Bowick, K. Freese, Phys. Lett. 138B, 159(1984).

Table 1

Process	Model	x	y	z
$q_i\bar{q}_i \to q_i\bar{q}_i$	1	3	3	0
	2	3	1	2
	3	3	3	0
	4	3	0	3

Values of the parameters appearing in 13–14 and 15. Equation 13–Diagonal interactions.

Process	Model	x_H	y_H	z_H	x_V	y_V	z_V
$u\bar{u} \leftrightarrow d\bar{d}$	1	0	0	0	3	0	3
$c\bar{c} \leftrightarrow s\bar{s}$	2	2	0	2	1	0	1
$t\bar{t} \leftrightarrow b\bar{b}$	3	0	0	0	3	0	3
	4	3	0	3	0	0	0
$u\bar{u} \leftrightarrow c\bar{c}$	1	2	2	0	1	0	1
$u\bar{u} \leftrightarrow t\bar{t}$	2	2	0	2	1	0	1
$c\bar{c} \leftrightarrow t\bar{t}$	3	3	3	0	0	0	0
$d\bar{d} \leftrightarrow s\bar{s}$	4	0	0	0	3	3	0
$d\bar{d} \leftrightarrow b\bar{b}$							
$s\bar{s} \leftrightarrow b\bar{b}$							
$u\bar{u} \leftrightarrow s\bar{s}$	1	0	0	0	1	0	1
$u\bar{u} \leftrightarrow b\bar{b}$	2	1	0	1	1	0	1
$c\bar{c} \leftrightarrow b\bar{b}$	3	0	0	0	0	0	0
$c\bar{c} \leftrightarrow d\bar{d}$	4	0	0	0	0	0	0
$t\bar{t} \leftrightarrow d\bar{d}$							
$t\bar{t} \leftrightarrow s\bar{s}$							

Equation 14 non-diagonal terms, $q_i\bar{q}_j \to q_i\bar{q}_j, i \neq j$.

Process	Model	x_H	x_V
$u\bar{c} \leftrightarrow d\bar{s}$	1	0	2
$u\bar{t} \leftrightarrow d\bar{b}$	2	0	0
$c\bar{u} \leftrightarrow s\bar{d}$	3	0	3
$c\bar{t} \leftrightarrow s\bar{b}$	4	3	0
$t\bar{u} \leftrightarrow b\bar{d}$			
$t\bar{c} \leftrightarrow b\bar{s}$			

Equation 15 Family conserving $q_i\bar{q}_j \to q_k\bar{q}_\ell$.

Figure Captions

Figure 1 — Duality diagram showing the process quark anti-quark → quark anti-quark via an s channel composite vector meson resonance.

Figure 2 — Diagram for the process quark anti-quark → gluon gluon.

Figure 3 — Diagram for the process gluon gluon → gluon gluon.

Figure 4 — Differential cross-section $d\sigma/dp_T/dy$ for the production of a jet at y = 0 in pp collisions at $\sqrt{s} = 40TeV$. The contributions of the different final states are shown seperately; quark-quark (dashed-line) gluon-quark (doted line), gluon-gluon (dot-dashed line) and the total (solid line). Model 1 is shown with the parameters, $g_p = 3,\ g_v = \sqrt{8\pi},\ M_v = 3TeV,$ c = 1.

Figure 5 — The differential cross-section $d\sigma/dp_t/dy$ for model 1 with M_v = 6, 10 and 30TeV, $g_p = 3, g_v = \sqrt{8\pi}$, c = 1. Also shown in the rate from pure QCD ($M_v = \infty$).

Figure 6 — As Figure 5 except for model 3 with $M_v = 3, 6, 10, 30TeV$.

Figure 7 — The differential cross section for model 1 with $g_p = 1, g_v = \sqrt{8\pi}, M_v = 3, 6, 10, 30TeV, \gamma = 0.2$

Figure 8 — As for Figure 7 except for model 2.

Figure 9 — As for Figure 7 except for model 3.

Figure 10 — As for Figure 7 except for model 4.

Figure 11 — The differential cross section $d\sigma/dM$ for the production of a jet pair of invarient mass M. Both jets satisfy $|y| < 1.5$. Model 1 is used with $M_v = 3, 6, 10, 30TeV, g_p = 1, g_v = \sqrt{8\pi}, c = 1, \gamma = 0.2$.

Figure 12 — As Figure 11 except that model 2 is used.

Figure 13 — As Figure 11, except γ= 0.5 is used.

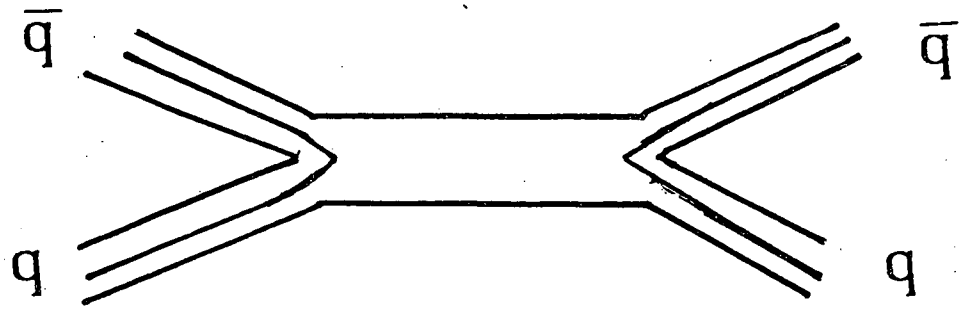

Figure 1

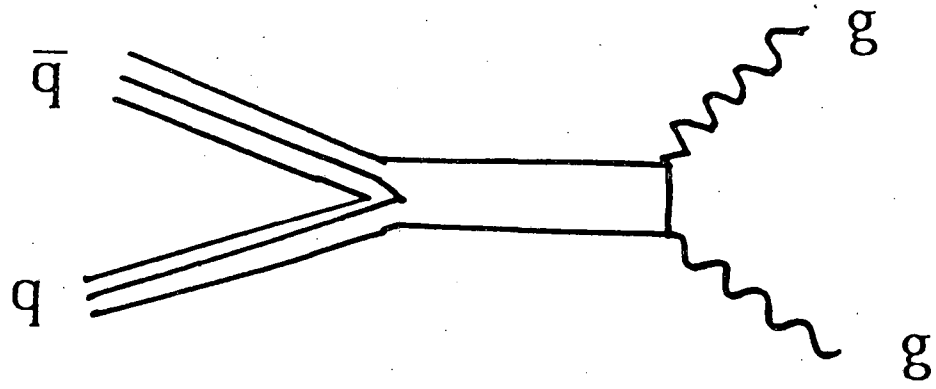

Figure 2

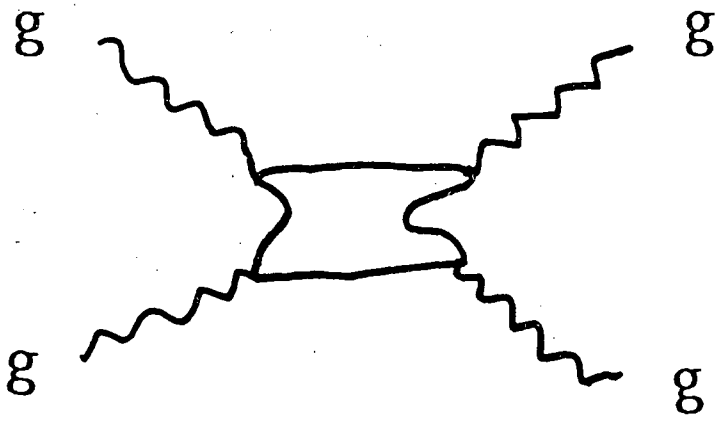

Figure 3

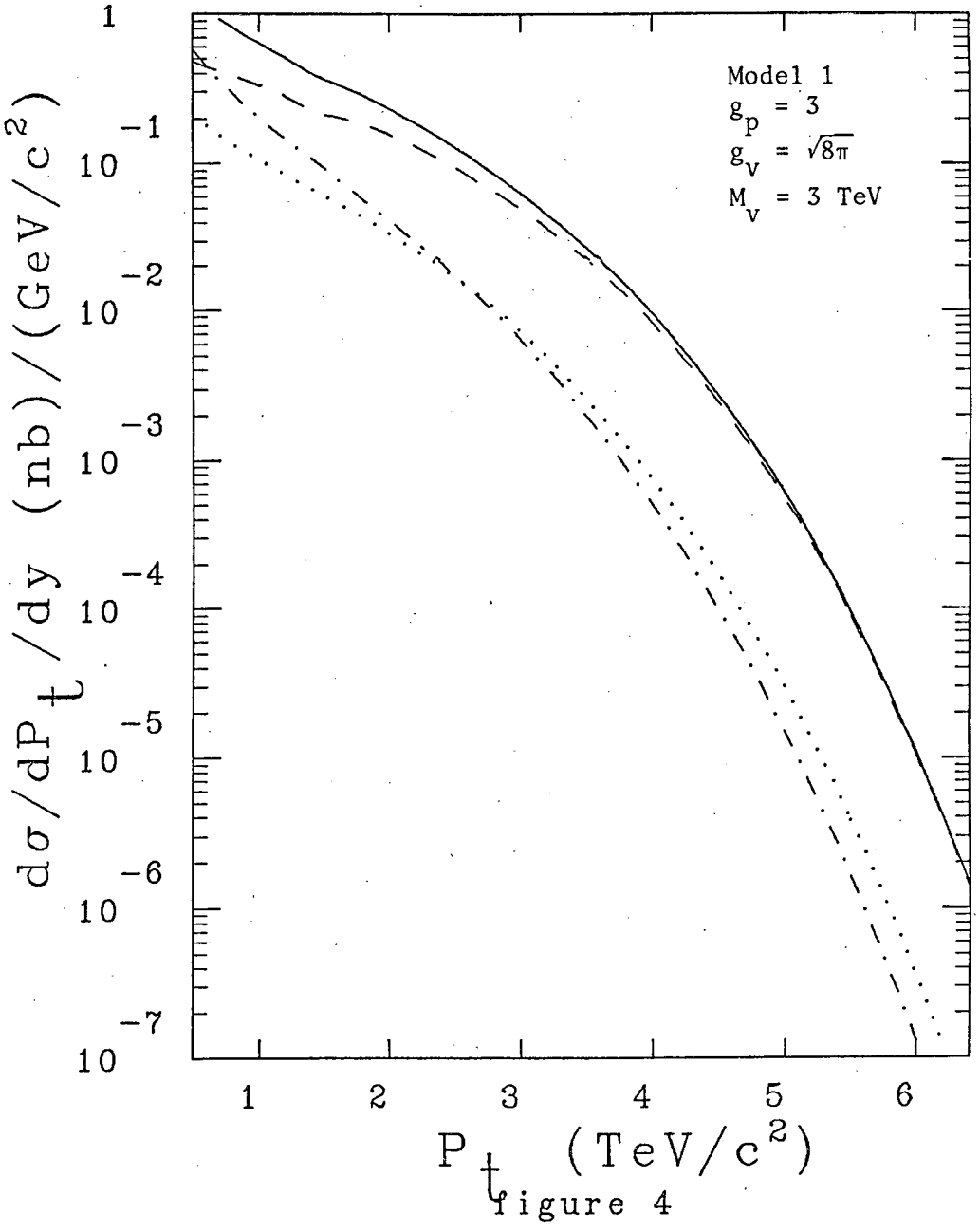
Model 1
g_p = 3
g_v = $\sqrt{8\pi}$
M_v = 3 TeV
$d\sigma/dP_t/dy$ (nb)/(GeV/c^2)
P_t (TeV/c^2)
1
10^{-1}
10^{-2}
10^{-3}
10^{-4}
10^{-5}
10^{-6}
10^{-7}
1
2
3
4
5
6

Figure 4

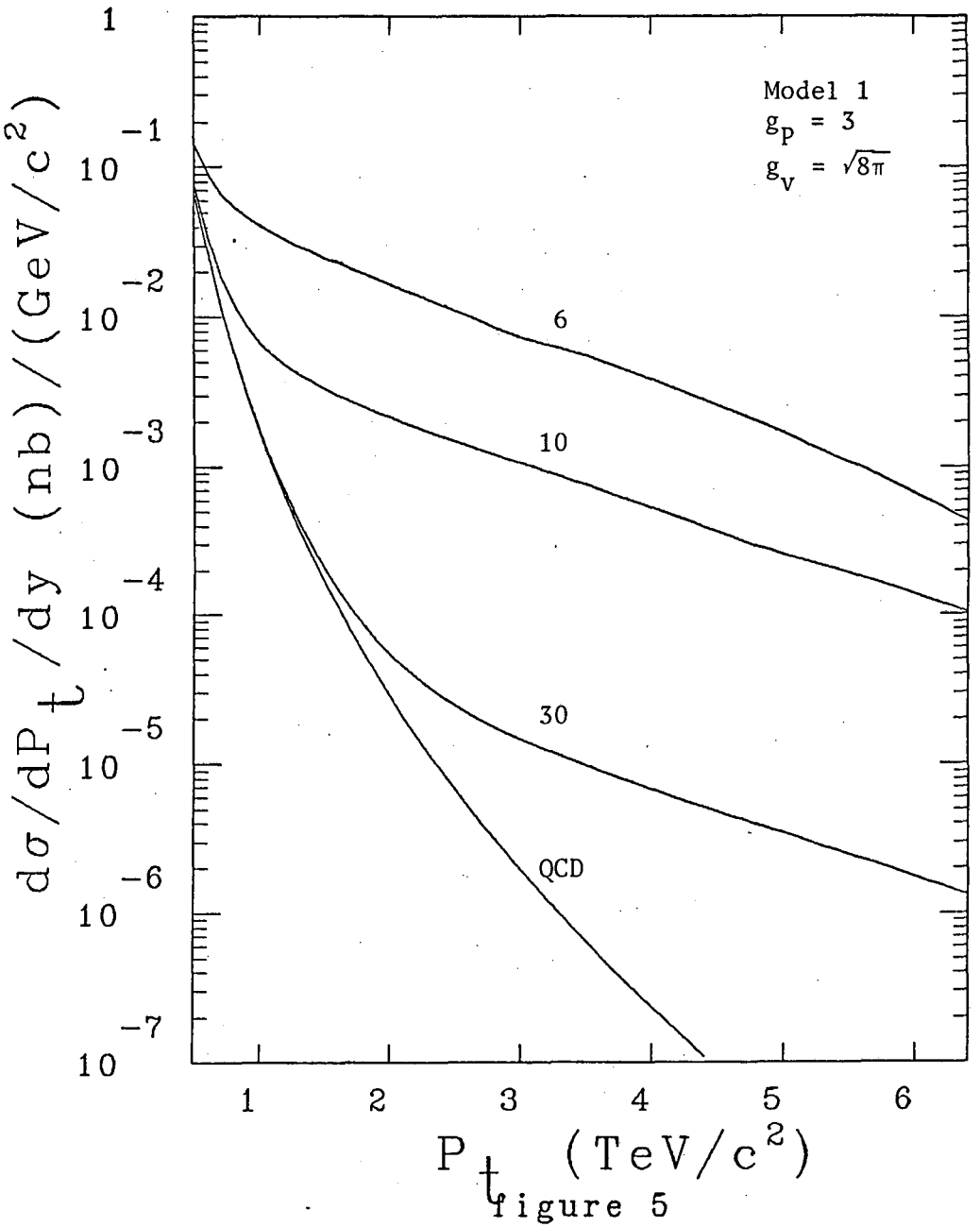
Model 1
g_p = 3
g_v = $\sqrt{8\pi}$
6
10
30
QCD
$d\sigma/dP_t/dy$ (nb)/(GeV/c^2)
P_t (TeV/c^2)
1
10^{-1}
10^{-2}
10^{-3}
10^{-4}
10^{-5}
10^{-6}
10^{-7}
1
2
3
4
5
6

Figure 5

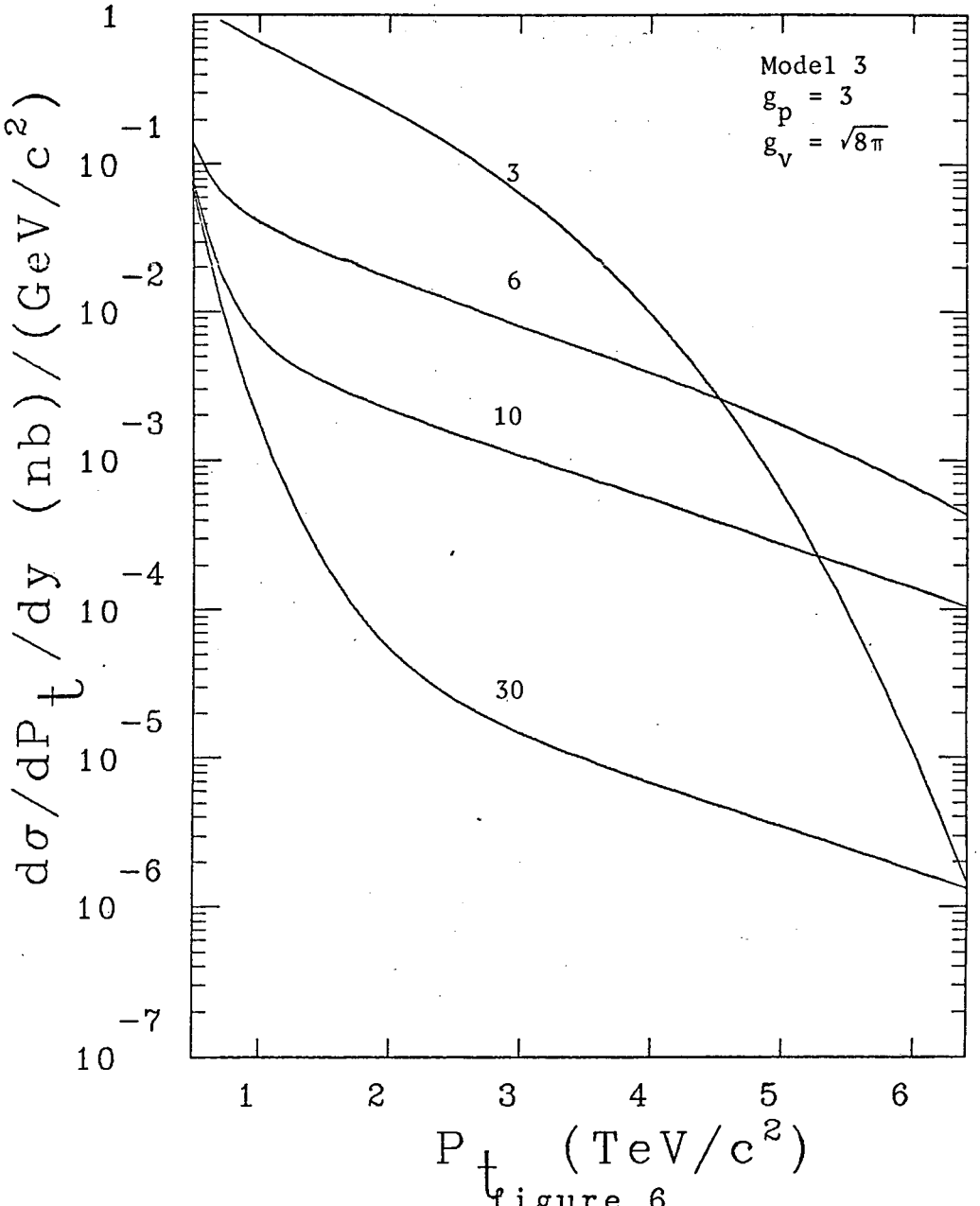
Model 3
g_p = 3
g_v = $\sqrt{8\pi}$
3
6
10
30
$d\sigma/dP_t/dy$ (nb)/(GeV/c^2)
P_t (TeV/c^2)
1
10^{-1}
10^{-2}
10^{-3}
10^{-4}
10^{-5}
10^{-6}
10^{-7}
1
2
3
4
5
6

Figure 6

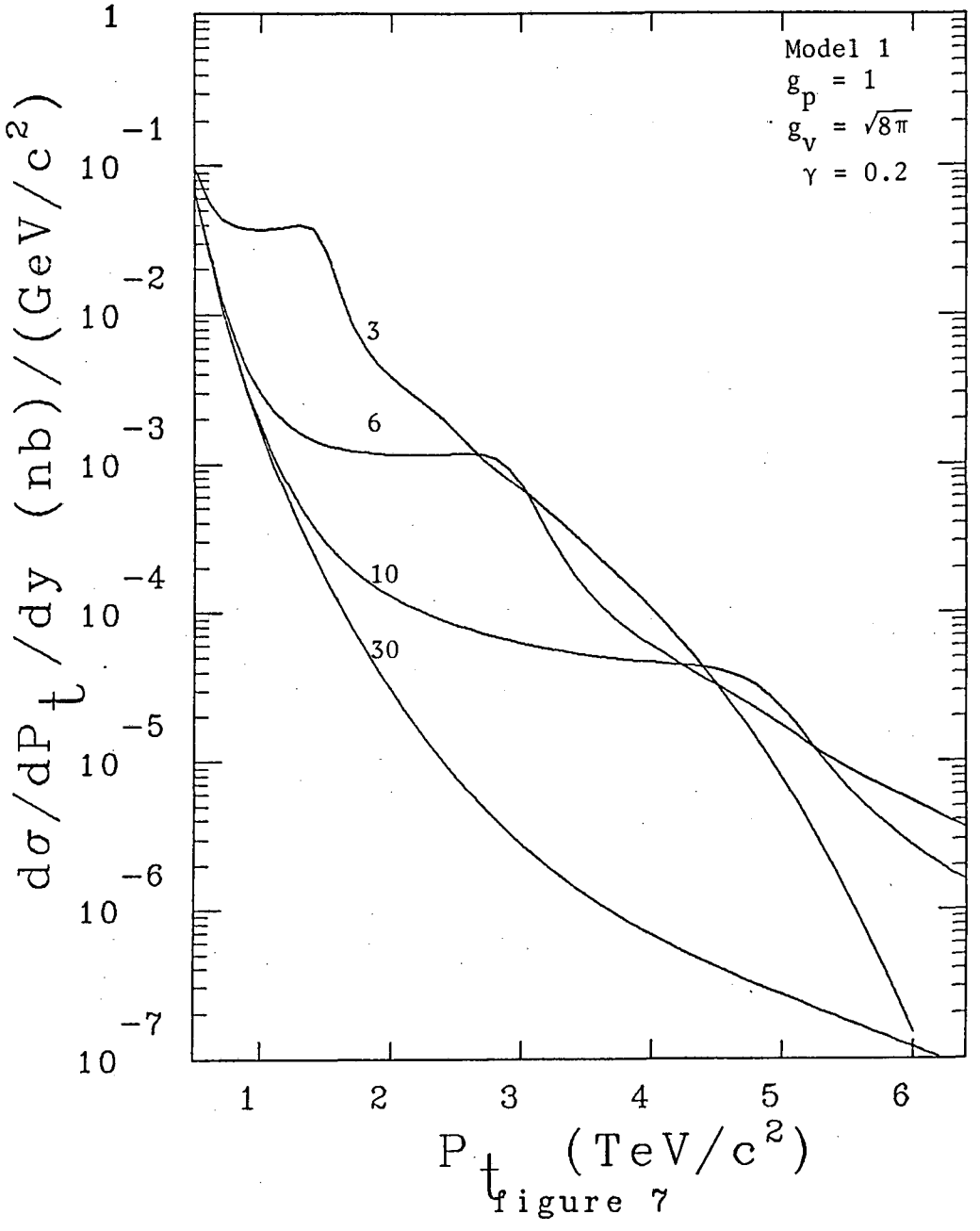
Model 1
g_p = 1
g_v = $\sqrt{8\pi}$
γ = 0.2
3
6
10
30
$d\sigma/dP_t/dy$ (nb)/(GeV/c^2)
P_t (TeV/c^2)
1
10^{-1}
10^{-2}
10^{-3}
10^{-4}
10^{-5}
10^{-6}
10^{-7}
1
2
3
4
5
6

Figure 7

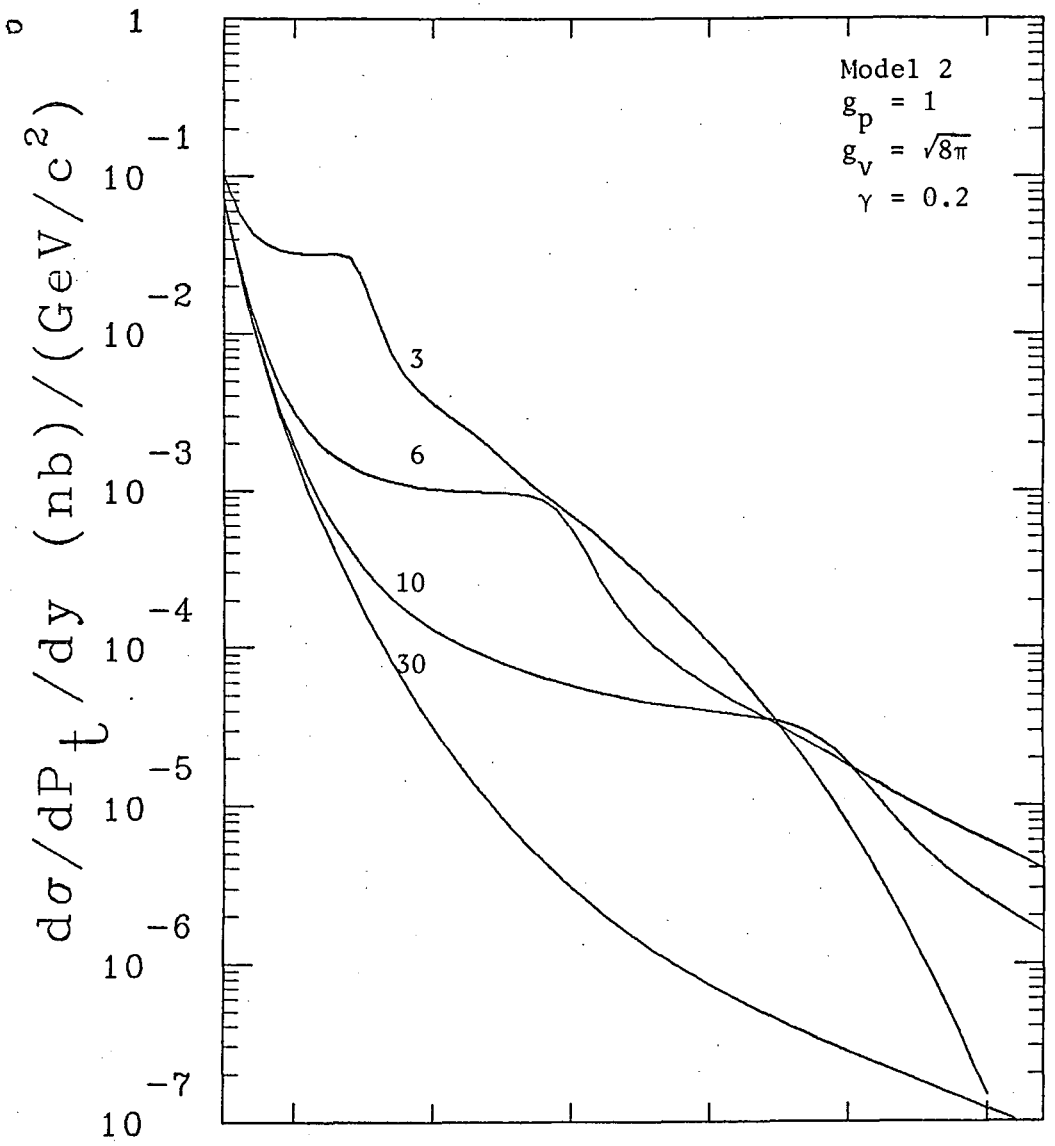
Model 2
g_p = 1
g_v = $\sqrt{8\pi}$
γ = 0.2
3
6
10
30
$d\sigma/dP_t/dy$ (nb)/(GeV/c^2)
P_t (TeV/c^2)
1
10^{-1}
10^{-2}
10^{-3}
10^{-4}
10^{-5}
10^{-6}
10^{-7}
1
2
3
4
5
6

Figure 8

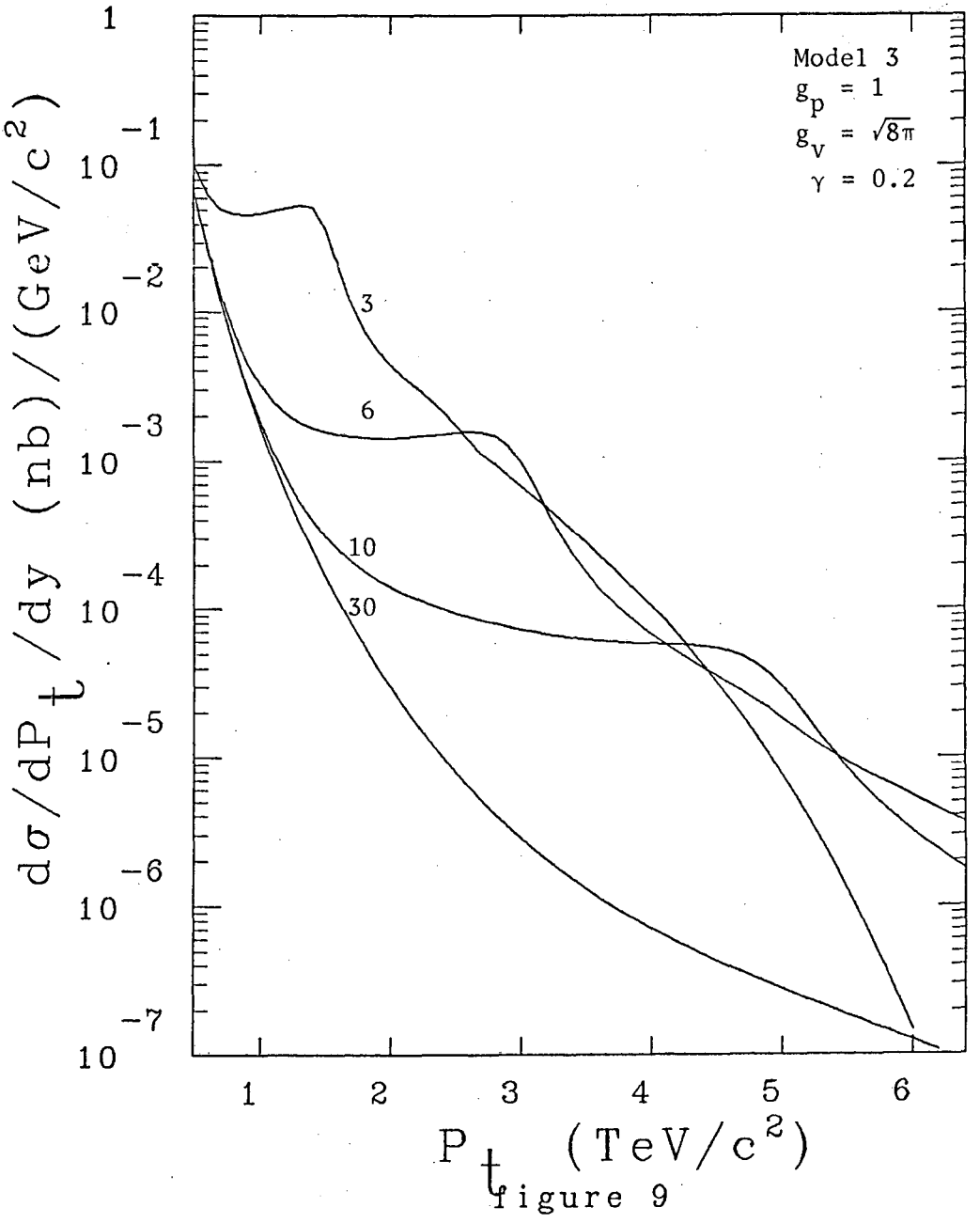
Model 3
g_p = 1
g_V = $\sqrt{8\pi}$
γ = 0.2
3
6
10
30
$d\sigma/dP_t/dy$ (nb)/(GeV/c^2)
P_t (TeV/c^2)
1
10^{-1}
10^{-2}
10^{-3}
10^{-4}
10^{-5}
10^{-6}
10^{-7}
1
2
3
4
5
6

Figure 9

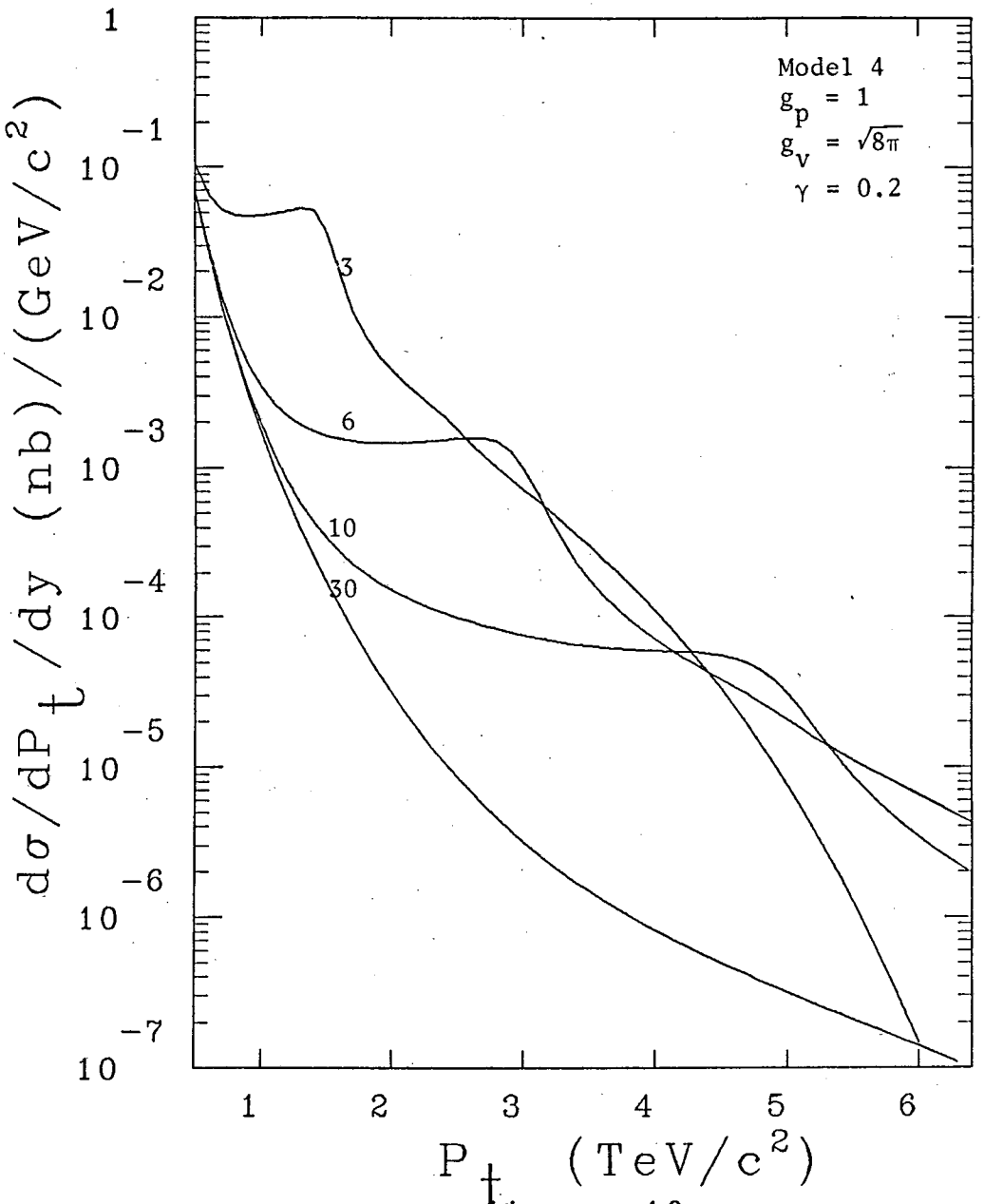
Model 4
$g_p = 1$
$g_v = \sqrt{8\pi}$
$\gamma = 0.2$
3
6
10
30
$d\sigma/dP_t/dy$ (nb)/(GeV/c^2)
P_t (TeV/c^2)
1
10^{-1}
10^{-2}
10^{-3}
10^{-4}
10^{-5}
10^{-6}
10^{-7}
1
2
3
4
5
6

Figure 10

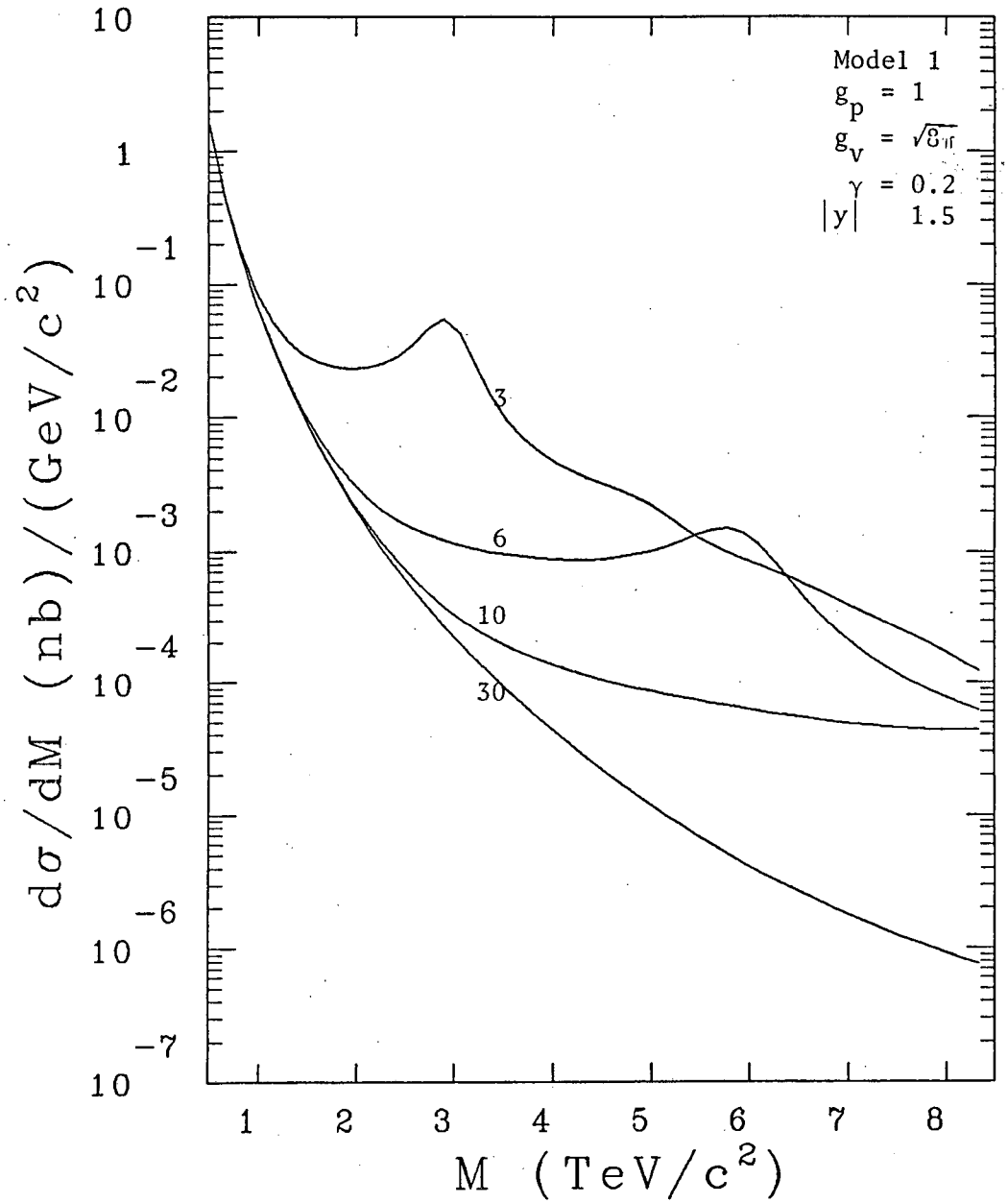
Model 1
g_p = 1
g_v = $\sqrt{8\pi}$
γ = 0.2
|y| 1.5
3
6
10
30
$d\sigma/dM$ (nb)/(GeV/c^2)
M (TeV/c^2)
10
1
10^{-1}
10^{-2}
10^{-3}
10^{-4}
10^{-5}
10^{-6}
10^{-7}
1 2 3 4 5 6 7 8

Figure 11

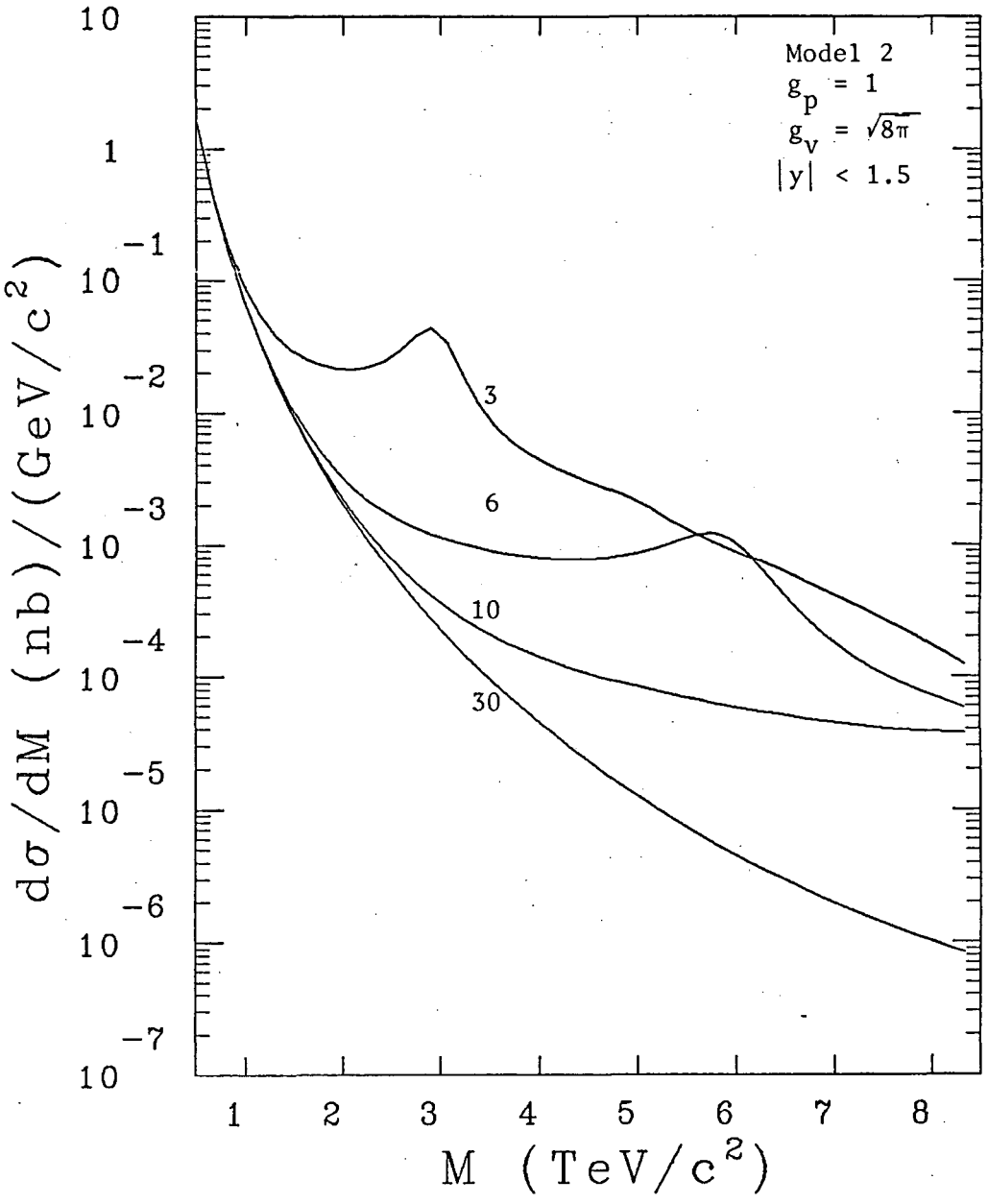
Model 2
$g_p = 1$
$g_v = \sqrt{8\pi}$
$|y| < 1.5$
3
6
10
30
$d\sigma/dM$ (nb)/(GeV/c^2)
M (TeV/c^2)
10
1
10^{-1}
10^{-2}
10^{-3}
10^{-4}
10^{-5}
10^{-6}
10^{-7}
1
2
3
4
5
6
7
8

Figure 12

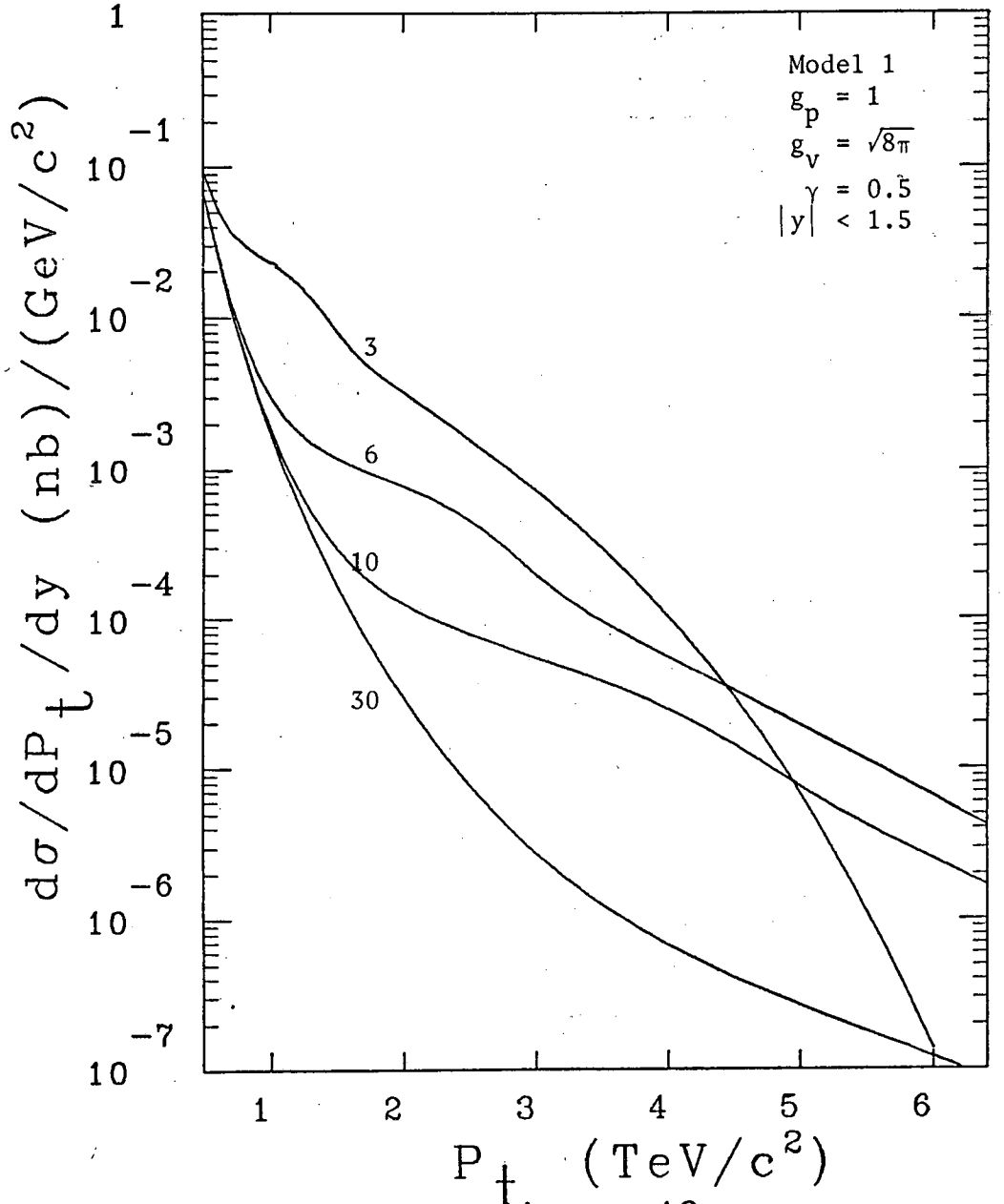
Model 1
g_p = 1
g_v = $\sqrt{8\pi}$
γ = 0.5
|y| < 1.5
3
6
10
30
$d\sigma/dP_t/dy$ (nb)/(GeV/c^2)
P_t (TeV/c^2)
1
10^{-1}
10^{-2}
10^{-3}
10^{-4}
10^{-5}
10^{-6}
10^{-7}
1
2
3
4
5
6

Figure 13

LAWRENCE BERKELEY LABORATORY
TECHNICAL INFORMATION DEPARTMENT
UNIVERSITY OF CALIFORNIA
BERKELEY, CALIFORNIA 94720